Published in final edited form as:
Ann Biomed Eng. 2013 June ; 41(6): 1217–1232. doi:10.1007/s10439-013-0759-9.

Improving Pharmaceutical Aerosol Delivery During Noninvasive Ventilation: Effects of Streamlined Components

P. Worth Longest[1,2,*], **Laleh Golshahi**[2], and **Michael Hindle**[2]

[1]Department of Mechanical Engineering, Virginia Commonwealth University, Richmond, VA

[2]Department of Pharmaceutics, Virginia Commonwealth University, Richmond, VA

Abstract

Aerosol delivery efficiency during noninvasive ventilation (NIV) is known to be low (~10%) and is associated with poor outcomes of aerosol therapy. The objective of this study was to demonstrate the benefit of redesigning ventilation circuit components using a streamlining approach to improve aerosol delivery during nasal high flow therapy in adults with a conventional-sized aerosol from a mesh nebulizer. The ventilation circuit consisted of a humidifier, mesh nebulizer, mixing T-connector (with 90° angle), 10 mm tubing, and nasal cannula interface. *In vitro* experiments and computational fluid dynamics analyses were used to evaluate depositional losses in a system of existing components and a newly proposed streamlined T-connector and cannula at flow rates of 30 and 45 LPM. Streamlined designs reduced deposition in the T-connector by a factor of 4. In the nasal cannula, the streamlined designs reduced depositional losses by factors of 1.25–2.0. With the streamlined designs, the highest emitted dose achieved was >40% for a conventional-sized aerosol at 30 LPM. Streamlined geometries offer an effective method to significantly improve the delivery of aerosols through components of NIV systems. This increase in delivery efficiency is important for new inhaled medications with narrow therapeutic windows, increased costs, or long delivery times.

Keywords

Nasal high flow therapy; high flow nasal cannula; pharmaceutical aerosols; respiratory drug delivery; mesh nebulizer; non-invasive ventilation; mechanical ventilation

INTRODUCTION

Noninvasive ventilation (NIV) is becoming increasingly popular to treat respiratory insufficiency caused by a number of sources, including sleep apnea, chronic obstructive pulmonary disease (COPD), and acute respiratory failure.[16,36] The delivery of pharmaceutical aerosols to patients receiving NIV has demonstrated a clear clinical benefit.[9,17] Bronchodilators and corticosteroids are often helpful for patients receiving NIV.[9,11,43] However, other envisioned medications for delivery during mechanical ventilation include antibiotics, prostanoids, mucolytics, and surfactants. Delivery during NIV is advantageous for medications that are rapidly cleared (e.g., prostanoids), require long-term delivery (e.g., mucolytics), or require high doses (e.g., surfactants and antibiotics). One promising form of NIV is nasal high flow therapy (HFT), which involves the continuous delivery of air or blended oxygen to the nose using a cannula interface.[12,37] The air is heated and humidified to improve comfort and allow for flow rates of 10–40 LPM in

*Corresponding author: Dr. P. Worth Longest, PhD, Virginia Commonwealth University, 401 West Main Street, P.O. Box 843015, Richmond, VA 23284-3015, Phone: (804)-827-7023, Fax: (804)-827-7030, pwlongest@vcu.edu.

adults.[7,37] Compared with mask delivery or usual care, patients receiving nasal HFT had improved blood oxygenation, respiratory rates, and quality of life scores.[37,39,41,42] Ideally, pharmaceutical aerosols can be delivered during nasal HFT without interrupting the continuous delivery of high flow oxygen to the patient. However, the delivery of an aerosol from the generation device through relatively narrow tubing and past a nasal cannula interface is extremely challenging due to depositional losses of drug aerosol droplets. In general, aerosol delivery through all forms of mechanical ventilation systems results in very high depositional drug losses,[10,11] and the associated low and variable doses received by the patient are sometimes blamed for unsuccessful therapies and failed clinical trials of new inhaled medications.[9,15]

For conventional aerosol therapy during NIV, drug delivery efficiencies through the ventilation circuit are typically <1–10% in adults and children based on *in vitro* experiments and 1–6% *in vivo*.[9,11] Differences between *in vitro* and *in vivo* estimates are often due to the absence of humidified conditions and the absence of an exhaled fraction in the *in vitro* experiments. Previous studies of aerosol delivery efficiency with nasal cannula interfaces have focused on low flow rates in adult and infant models.[3,4] Bhashyam et al.[4] considered aerosol delivery from a mesh nebulizer (Aeroneb Solo, Aerogen Limited, Galway, Ireland) through infant, pediatric, and adult nasal cannulas at an inspiratory flow rate of 3 LPM with a heated and humidified system. Depositional losses in the connectors, tubing, and cannula resulted in a total output that ranged from 19–27% of the initial dose when simulated inhalation was included in the system. Ari et al.[3] considered aerosol delivery from the Aeroneb Solo device through an Optiflow (Fisher and Paykel, Irvine, CA) pediatric nasal cannula at flow rates of 3 and 6 LPM with oxygen or heliox. The maximum cannula aerosol delivery efficiency of approximately 10% occurred with a flow rate of 3 LPM and was decreased significantly with the use of the higher flow rate and heliox.

A number of studies have evaluated or reviewed factors influencing aerosol delivery during NIV and best practices for aerosol therapy administration.[2,9–11,17] These factors include ventilator parameters, breathing variables, interface selection, the circuit, the aerosol generation device, the drug, and patient interactions.[11,17] Current studies typically compare the performance of existing devices and selection of delivery parameters. For example, there is extensive literature on the performance of metered-dose inhalers vs. nebulizers used during mechanical ventilation and the effects of different locations in the circuit for aerosol administration.[2,9,11] However, very few studies have considered redesigning components of the ventilator circuit to improve aerosol delivery without interfering with gas exchange. It is expected that a majority of deposition occurs in regions of sudden change to the flow passage, like sudden contractions, expansions, and direction change. Ivri et al.[18] suggested that low angles (< 15 degrees) could be used to improve aerosol delivery through ventilation circuits. However, this requires additional lengths in the ventilation tubing and components, and large overall changes in line direction (e.g., 90° and above) frequently cannot be avoided. In contrast, streamlining of individual components within the delivery circuit has previously not been explored. Streamlining involves the redesign of system components to smooth sudden changes in diameter and applies a radius of curvature to smooth changes in direction. The result is significantly more uniform flow with less flow separation, detachment, recirculation, vorticity, turbulence, and aerosol deposition by inertial impaction.

The objective of this study is to demonstrate the benefit of redesigning key ventilation circuit components for aerosol delivery during nasal HFT in adults with a conventional-sized aerosol (MMAD ~ 3–7 μm) from a mesh nebulizer. This system represents one of the most challenging cases for aerosol delivery during NIV due to the use of high flow rates (~ 30 LPM) and small diameters of the nasal cannula. From a practical standpoint, it is not possible to implement low angles in this system. The ventilation circuit consists of a

humidifier, mesh nebulizer, mixing T-connector (with 90° angle), 10 mm tubing, and nasal cannula interface. Both *in vitro* experiments and computational fluid dynamics (CFD) analyses are used to evaluate depositional losses using existing components and the newly proposed streamlined T-connector and cannula interface.

METHODS

NIV System Components

To generate a consistent high quality aerosol of conventional size, vibrating mesh nebulizer technology was selected. The Aeroneb Lab nebulizer (Aerogen Limited, Galway, Ireland) was implemented, which was previously characterized in the study of Longest et al.[26] Based on this previous study, the Aeroneb Lab device has a liquid aerosolization rate of 0.2 ml/min, an initial aerosol MMAD of 3.9 μm, and a particle number concentration of 4.28×10^5 part/cm^3 in an airflow of 15 LPM. The size of the Aeroneb Lab aerosol is smaller than the Aeroneb Pro commercial device, as well as other available mesh nebulizer devices, and this relatively small aerosol size is expected to minimize deposition and maximize the dose that passes through the NIV system.

The mesh nebulizer is coupled to the patient delivery tubing using a T-connector. In this study, 10 mm ventilator tubing was selected as a practical maximum that could be used with a nasal cannula interface. The commercially available T-connector for coupling the Aeroneb series of mesh nebulizers with 10 mm tubing is the neonate design. The neonate T-connector is illustrated in Figure 1a and features a 22 mm top inlet to accommodate the Aeroneb mesh nebulizer, a 9 mm air inlet, and a 10 mm air outlet. Length of the air outlet available for particle deposition in the T-connector depends on the insertion depth of the tube and in this study was 5 mm. The component naming convention in this study is based on the device design - tubing size - and type of component. The name Base-10-T indicates a commercial (base) design, compatibility with 10 mm tubing, and a T-connector component.

To redesign the Base-10-T component for efficient aerosol delivery at flow rates consistent with HFT, a streamlined design was developed, as illustrated in Figure 1b. The streamlined T-connector allows for insertion of the Aeroneb mesh nebulizer as with the commercial unit. Preliminary CFD simulations were used in order to minimize deposition within the streamlined T-connector. Based on these simulations, it was determined that the final design should maintain velocity within the mixing region below 2 m/s and should eliminate recirculation along the top of the T-connector downstream of the nebulizer. The final streamlined design uses gradual size change from the inlet 10 mm tubing through a larger 24 mm internal diameter and back through the 10 mm outlet. The sigmoid curves at the inlet and outlet of the streamlined T-connector have radii of curvatures of approximately 18 and 22 mm, respectively. The larger diameter of the T-connector allows more room for the aerosol to change direction without striking a surface. The outlet tube of the streamlined T-connector is in-line with the top of the main flow passage, which minimizes recirculation in this key region. A smoothed connection is used to join the Aeroneb branch with the main flow passage. Implementation of this smoothed connection reduces turbulence generation sites, flow detachment, and recirculation. Finally, a perforated plate is used to unify the inlet flow and produce a more unidirectional stream through the entrainment region below the nebulizer. Unifying the flow refers to reducing velocity gradients and regions of recirculation that can enhance particle deposition. The perforated plate contained 32 holes with diameters of 2 mm, which was found to unify the downstream flow without excessively increasing turbulence. The result is the streamlined (SL) and perforated (p) design, denoted SLp-10-T, which has a total length of 12 cm. As an alternative, a fin design was used to unify the inlet flow, illustrated as the insert in Figure 1b. Circular fins were implemented along with a filled central region with the intent of eliminating a central jet moving through

the entrainment region and resulting in the SLf-10-T design. In the rapid prototyped experimental design, thin (1 mm) crosspieces were used to hold the circular fins in place, which were not included in the CFD geometry and are not shown in Figure 1b.

For the nasal cannulas, 10 mm tubing was again selected along with conventional large bore nostril prongs. The Optiflow (Fisher and Paykel, Irvine, CA) nasal cannula was selected as the base case, which was also considered in the aerosol delivery study of Ari et al.[3] In the current study, the medium-sized adult Optiflow cannula was evaluated with a 10 mm inlet line and approximate outlet prong diameter of 5 mm (Base-10-CL; Fig. 1c). The connective tubing was 20 cm in length with an internal diameter of 10 mm. To create a more realistic delivery scenario compared with straight tubing, a gradual 90° bend of the tube was employed, as illustrated in the figure. The cannula outlets form an approximately 60° angle with a horizontal plane. To navigate the delivery circuit, the aerosol must transverse a 90° bend in the T-connector, a 90° bend in the connective tubing, turn 90° to enter the cannula prongs, and finally turn an additional 60° to enter the nose. The resulting 330° in aerosol direction change is significantly greater than the 15° maximum specified by Ivri and Fink.[18]

The streamlined cannula design has a single 10 mm inlet and smoothed elliptical flow passage for the aerosol to enter the left or right nostril (Fig 1d). Again, preliminary CFD simulations were used to understand the flow field and minimize flow features that contributed to deposition. The division point of the two nostril prongs was selected at a position that evenly divided the flow between the left and right nostrils. This streamlined cannula also includes nasal prongs containing oval outlets with major and minor diameters of 7.5 and 5 mm, respectively. The oval shape is expected to reduce recirculating velocity in the cannula and exit velocities at the nose. The flow passages have radii of curvatures in the range of 10–13 mm with a distance of 14 mm between the nasal prongs centers. The streamlined cannula (SL-10-CL) has a diameter reduction from the 10 mm inlet tubing to 8 mm in the main cannula passage, which is part of a quick-connect design. The previous study of Longest et al.[30] considered a single aerosol inlet divided flow cannula and primarily submicrometer particles for enhanced condensational growth (ECG) delivery. In the current study, conventional aerosols are considered with a two pronged streamlined design.

Combinations of NIV Components

Different combinations of the base and streamlined components were assembled to determine deposition within individual components and total drug throughput, i.e., emitted dose, for a composite NIV system. Considering the application of nasal HFT in adults, typical flow rates of 30 and 45 LPM through the system were evaluated. Reducing the flow rate below 30 LPM will improve aerosol throughput but may also diminish oxygen delivery during HFT and potentially reduce lung function. Individual cases considered in this study are described in Table 1. Briefly, Case 1 combines the commercial T-connector and cannula elements, Cases 2 and 3 consider the streamlined components, and Case 4 tests performance of the Optiflow cannula with a streamlined T-connector. These four cases were evaluated at 30 LPM in the *in vitro* experiments as well as 30 and 45 LPM with CFD simulations.

It is important to note that the base neonatal T-connector was initially intended for low flow delivery. Furthermore, the Optiflow nasal cannula is a gas-delivery device and was not designed for aerosol delivery. These selected existing components are likely the best case for delivering a conventional aerosol during HFT using off-the-shelf items. However, from previous studies it is expected that delivery efficiency of the existing components will be very low at flow rates of approximately 30 LPM and above. Based on this expected low delivery and a lack of suitable alternatives, aerosols are typically not delivered during HFT in a clinical setting. The current study seeks to demonstrate that improved delivery can be achieved using a streamlining approach compared with the base components as a control.

This approach is also relevant to general aerosol delivery during mechanical ventilation where system components are typically designed for effective gas delivery but have very high depositional losses with aerosols.

Experimental Procedure - Overview

In vitro experimental studies were used to evaluate the initial size of the aerosol exiting the Aeroneb Lab nebulizer in the absence of the NIV setups and to determine aerosol deposition in each component of the delivery system as well as total throughput, or emitted dose, for Cases 1–4 at 30 LPM. In all experiments, the drug formulation was aqueous-based with 0.2%w/v albuterol sulfate (AS) in deionized water. The Aeroneb Lab nebulizer was operated for 30 s resulting in an average nominal dose of approximately 463 μg of drug (with the average value range of 447–494 μg for the four cases studied).

Experimental Procedure - Particle Sizing

To verify the aerodynamic particle size distribution of the aerosol produced by the Aeroneb Lab nebulizer, a set of experiments was conducted in which the nebulizer was actuated directly into an Andersen Cascade Impactor (ACI; Graseby-Andersen Inc., Smyrna, GA). Previous estimates of aerosol size from the Aeroneb Lab nebulizer were based on the use of a 22 mm T-connector with radial dilution using room air at 28.3±2 LPM. In the current study, the nebulizer and ACI were placed in an environmental cabinet (Espec, Hudsonville, MI) and maintained at 25 °C and 93% RH. A gap distance of approximately 10 mm separated the nebulizer outlet and the ACI inlet, allowing for the entrainment of humidified air at a rate of 28.3±2 LPM. Constant temperature and near-saturated relative humidity conditions prevented size change of the aerosol arising from unwanted evaporation and condensation.

Experimental Procedure - Deposition

In order to determine drug mass deposition in Cases 1–4, rapid prototyped models of the streamlined components were constructed. Specifically, a Viper SLA system (3D Systems, Valencia, CA) was used to construct the streamlined T-connector and cannula designs using Accura 60 clear plastic resin. The connective tubing was standard corrugated ventilator line with a measured internal diameter of 10 mm (Instrumentation Industries, Bethel Park, PA). The experiments were conducted at room temperature (23–25 °C). The inlet airflow was heated and humidified to 25 °C and 93% RH using a Vapotherm 2000i HFT unit (Vapotherm Inc., Stevensville, MD). Humidifying the inlet airstream was used to avoid aerosol evaporation and is consistent with nasal HFT gas delivery. The *in vitro* deposition experiments were conducted at a steady state flow rate of 30 LPM. Aerosol exiting the cannula for Cases 1–4 (Table 1) was captured on a filter and used to determined aerosol mass balance relative to the nominal dose.

Drug deposition on the nebulizer, T-connectors, tubing, cannulas, filter and on the ACI collection plates for the initial size experiment was determined following collection of washings using appropriate volumes of deionized water (10–20 ml). The solutions were then assayed using a validated HPLC-UV method for AS. In the aerosol sizing experiments, the mass of AS on each impaction plate was determined and used to calculate the aerodynamic particle size distribution of the drug. The mass median aerodynamic diameter (MMAD) was defined as the particle size at the 50th percentile on a cumulative percent mass undersize distribution (D50) using linear interpolation. The mass of formulation nebulized was determined by weighing the nebulizer before and after each experiment. The solution AS concentration and the mass of formulation nebulized were used to determine the nominal dose of AS delivered. AS system deposition results were reported as a percentage of the nominal delivered dose. At least four replicates of each experiment were performed.

CFD Simulations - Transport Models

Computational fluid dynamics simulations were conducted to guide the initial development of the streamlined designs, demonstrate the improved flow characteristics of the streamlined models, and predict aerosol deposition in each component of the systems. Blunt inlet flow profiles were assumed to enter the T-connectors at least 10 tube diameters upstream. Isothermal, incompressible, and constant-property flow was assumed in all cases. For inlet flow rates of 30 and 45 LPM, the characteristic Reynolds numbers in 10 mm tubing are 4051 and 6076, respectively, which indicate turbulent flow and the potential for turbulent aerosol dispersion. Turbulence in the components will be amplified in the presence of changes in flow direction and constrictions.

The flow fields in each component were solved using Fluent 12 (Ansys Inc., Canonsburg, PA) with a steady or transient solution and the low Reynolds number (LRN) k-ω two-equation turbulence model. This turbulence model was selected based on its accuracy combined with high efficiency compared with more complex methods, such as large eddy simulation (LES). The LRN k-ω model was previously demonstrated to accurately estimate pressure drop, velocity profiles, and shear stress for transitional and turbulent flows.[13,46] Considering aerosol transport, the LRN k-ω model was previously shown to accurately predict particle transport and deposition for both monodisperse and polydisperse aerosol distributions in airway models and delivery devices on a regional and highly localized basis.[20,23,29,47]

Droplet trajectories were considered in each of the NIV circuit components to evaluate deposition and improvements associated with the streamlined designs. Monodisperse aerosol sizes of 3.9 μm and 4.7 μm were considered, which are consistent with the expected MMADs of aerosol generated by the Aeroneb Lab and Aeroneb Pro devices, respectively.[26] To accurately predict individual droplet trajectories and deposition within each system component, a Lagrangian tracking algorithm was employed. The Lagrangian transport equations are expressed

$$\frac{dv_i}{dt}=\frac{f}{\tau_d}(u_i-v_i)+g_i(1-\alpha) \quad \text{and} \quad \frac{dx_i}{dt}=v_i(t) \quad (1)$$

Here v_i and u_i are the components of the droplet and local fluid velocity, g_i denotes gravity, and α is the ratio of air to droplet density ρ/ρ_d. The characteristic time required for a droplet to respond to changes in fluid motion, or the droplet relaxation time, is expressed as $\tau_d=\rho_d d_d^2/18\mu$, where d_d is the droplet diameter and μ is the absolute viscosity. The pressure gradient or acceleration term for aerosols was neglected due to small values of the density ratio.[25] The drag factor f, which represents the ratio of the drag coefficient to Stokes drag, was based on the expression of Morsi and Alexander.[35] To model the effects of turbulent fluctuations on droplet trajectories, a random walk method was employed.[6,14,34] A near-wall anisotropic correction to turbulent particle dispersion was also included.[22,33]

CFD Simulations - Mesh Generation

Computational grids of the airflow passages were constructed based on previously established best practices. Hexahedral elements were used wherever possible, based on the findings of previous studies.[28,45] Tetrahedral and wedge elements were required to resolve flow around the perforated inlet plate. For the hexahedral mesh, near wall mesh size was typically smaller than 0.1 mm. For the tetrahedral grids in the vicinity of the inlet plate, near-wall mesh size was set at a constant 0.05 mm. The resulting four meshes had cell numbers ranging from 200,000 to 1,200,000. Grid convergence of these meshes was

established by comparing with meshes containing at least 30% more cells in each case. These comparisons indicated that there were minimal differences (< 5% relative error) in the maximum velocity and particle deposition values. As a result, the coarser meshes were considered sufficient and used in all subsequent simulations.

CFD Simulations - Numerical Solution

The CFD package Fluent 12 was used to solve the flow field and particle trajectory equations in each of the inhalers. User-supplied Fortran and C programs were used for the calculation of initial flow and particle profiles, near-wall anisotropic turbulence approximations, and near-wall particle interpolation.[31] All transport equations were discretized to be at least second order accurate in space. For the convective terms, a second order upwind scheme was used to interpolate values from cell centers to nodes. The diffusion terms were discretized using central differences. The particle trajectory solution was calculated using 4th-order Runge Kutta with an error control routine.[25] For the T-connector and cannula geometries, 3,000 and 6,000 particles were considered, respectively. Simulating additional particles had a negligible effect on impaction results in terms of deposition fraction.

Deposition Reporting

Deposition within individual components of the NIV system can be reported as a deposition fraction or deposition efficiency. The deposition fraction (DF) for a specific component of the NIV system is computed

$$DF_{component} = \frac{mass\ of\ drug\ deposited\ in\ component}{mass\ of\ drug\ entering\ system\ from\ nebulizer} \quad (2)$$

The corresponding deposition efficiency (DE) for an individual component is

$$DE_{component} = \frac{mass\ of\ drug\ deposited\ in\ component}{mass\ of\ drug\ entering\ component} \quad (3)$$

To determine the total deposition fraction in the system, DFs of individual components can be directly summed. Deposition efficiency values are convenient for determining how an individual component is performing without the influence of upstream components. Experimental deposition results are typically reported as DFs based on the nominal inlet dose from the nebulizer, which can be converted to DEs as

$$DE_{component} = \frac{DF_{component}}{IF_{component}} \quad (4)$$

where $IF_{component}$ is the inlet fraction of drug entering a component and is calculated as

$$IF_{component} = 1 - \sum DF_{previous\ components} \quad (5)$$

The emitted dose percentage is the fraction of drug that exits the system and is calculated as

$$Emitted\ dose\ \% = \left(1 - \sum DF_{all\ components}\right) \times 100\% \quad (6)$$

By considering both DF and DE values, the performance of individual system components can be evaluated along with the emitted dose to the patient. These deposition values are converted to percentages using a multiplication factor of 100 in the Results. In the CFD analysis, separate simulations were conducted for the five individual components shown in Figure 1. Deposition fractions in the components and in the combined systems (Table 1) along with emitted dose were then calculated using the formulas shown above for comparisons with the experiments. This approach may have a small effect on predicted deposition and emitted dose considering that the inlet conditions to the cannula tubing were approximated as uniform flow and particle profiles.

RESULTS

In Vitro Experiments

Based on cascade impaction with the ACI, the aerosol from the Aeroneb Lab nebulizer was found to have an initial mean MMAD (and standard deviation; SD) of 4.84 (0.26) μm with a geometric standard deviation of 5.7. This was surprisingly larger than the 3.9 μm MMAD previously measured in the study of Longest et al.[26] Differences in aerosol size may result from variability between individual Aeroneb Lab devices, change of the mesh nebulizer over time with use, and the method of sampling the aerosol. As described in the Methods section, the previous study of Longest et al.[26] used a T-connector to direct the aerosol into the impactor. Both deposition in the T-connector and connective tubing could have resulted in the previous lower measured aerosol size. In the current study, one Aeroneb Lab nebulizer was used to conduct all *in vitro* sizing and deposition experiments.

Experimentally determined DFs and emitted dose as a percentage of nominal dose, as well as standard deviations (SD), are presented in Table 2 for Cases 1–4. Deposition fractions in the nebulizer are low for all cases, which represents the drug mass deposited in the nebulizer unit downstream of the vibrating mesh. Considering the T-connectors, the highest deposition is observed in the Base-10-T design (30.6%), which is reduced to approximately 5% with both of the streamlined options. Deposited drug is also high in the 10 mm diameter tubing, which is an unavoidable result of using conventional-sized aerosols during NIV delivery. Based on the use of DFs, it is difficult to evaluate performance of the cannula designs because the reported values are influenced by different percentages of upstream deposition. However, Cases 2 and 4 use the same SLp-10-T design with the SL and Base-10-CL cannulas, respectively. Considering this comparison, the SL-10-CL design used in Case 2 clearly has lower drug deposition compared with the Base-10-CL design of Case 4. Large improvements in measured emitted doses are observed for the streamlined designs, with Case 2 having a maximum value of 44%.

Deposition efficiency values determined from the *in vitro* experiments and calculated using Eq. (4) are reported in Table 3 for Cases 1–4. Relative percent differences in DE and emitted dose are also provided in Table 3, which are calculated with respect to Case 1, as defined in the table. Negative percent differences represent a reduction in DE or emitted dose relative to Case 1. Considering the T-connector at 30 LPM, the streamlined designs in Cases 2–4 reduce deposition by approximately −70% (or a factor of 4×) compared with Case 1. Deposition efficiencies in the tubing are similar for all four cases. Considering the cannula, Cases 2 and 3 indicate that the SL-10-CL design reduces deposition compared with Base-10-CL by approximately −15 to −20%. Considering the emitted dose, Case 2 provides a near 60% increase that illustrates a large improvement in the dose delivered using the streamlined designs compared with Case 1. Case 4 provides a 20% relative difference in emitted dose compared with Case 1, indicating that there is an improvement in dose delivery when the SLp-10-T connector is combined with the commercially available Base-10-CL cannula.

CFD Visualization of the Flow Field

CFD simulations of the flow field in each component at a steady state flow rate of 30 LPM are presented in Figure 2. In this figure, the flow field is sampled at select planes, contoured based on local speed, and streamlines are used to visualize the flow motion. Considering the T-connectors, the narrow inlet tube and sudden expansion of the Base-10-T model creates a high velocity jet of airflow moving through the design (Figure 2a). This relatively high velocity induces recirculation both in the nebulizer region of the geometry and in the entrainment region, which will likely make it difficult for the aerosol to enter the airstream and leave the connector. Both the sudden contraction and sudden expansion of the Base-10-T design as viewed by the airstream serve as sites of additional turbulence generation.

The SL-10-T geometry is observed to lower overall velocity values through the use of gradual expansions and contractions (Figure 2b). Reduced recirculation in the nebulizer region is observed compared with Case 1 (Figure 2a). The perforated plate creates a region of vortical flow immediately downstream of this structure. However, the flow is unified and one-directional once it enters the entrainment region below the nebulizer. Finally, the off-center placement of the outlet tube eliminates a recirculation region along the top of the device downstream of the T-connector, which was observed with other prototyped versions in the development process (not shown).

Comparing the nasal cannula designs (Figure 2c vs. d), largely reduced velocity values are observed with the streamlined model. These reduced velocity values are particularly important in the small diameter prong region, where deposition by impaction is expected to be the highest. The streamlined design also eliminates a recirculation region observed on the downstream side of the cannula body in Base-10-CL. The contour plots in Figure 2 include the numerical outlet region extending beyond the exit of the cannulas, which is required for a high quality CFD solution of the flow field.

Trajectories of 3.9 μm droplets in each of the components, colored based on local velocity, are illustrated in Figure 3. Considering the T-connectors, higher droplet deposition velocities, more recirculation in the entrainment region, and increased turbulent dispersion are observed with the base model compared with the streamlined design (Figure 3a vs. b). For the SL-10-T component, the aerosol is efficiently entrained and moves predominately downstream with little recirculation and chance for deposition. As expected for the cannula, lower velocities are observed in the trajectories for the streamlined design in the region of the nasal prongs (Figure 3c). As a result, the trajectories tend to exit the Base-10-CL model through the right hand side of the prongs, whereas they are centered in the nasal prongs of the streamlined design (Figure 3d). Some trajectories are also observed in the recirculation region of the Base-10-CL design.

CFD Predictions of Deposition

CFD simulations of both 3.9 μm and 4.7 μm monodisperse droplets were considered at flow rates of 30 and 45 LPM. For the experimental flow condition of 30 LPM, deposition results for both monodisperse particle sizes were compared with the experimental data. It was determined that the 4.7 μm monodisperse aerosol best approximated the experimental conditions. Table 4 provides a comparison of deposition efficiencies and emitted doses for the *in vitro* experiments and CFD simulations with a 4.7 μm aerosol at 30 LPM. In general, the monodisperse CFD estimates agree relatively well with the *in vitro* results. As the polydisperse aerosol travels through the system in the experiments, its aerodynamic size is reduced as larger particles are more likely to deposit. Therefore, the CFD estimates with a fixed particle size tend to under-predict deposition in the T-connector and over-predict

deposition in the tubing and cannula. Nevertheless, DE estimates are typically within 30% relative difference of the experiments in each component.

Emitted doses are also compared between the model and experiments in Table 4. The experimental emitted dose is based on the total experimental DF from Table 2 subtracted from 100%. Predicted emitted doses are within a relative difference of about 10% or less for Cases 2 and 3 compared with the measured value and within about 30% for Case 1 compared with the experimental value. As a result, the CFD predictions for emitted dose also appear reasonably accurate taking into account the use of a monodisperse aerosol and the potential for experimental variability and some error.

Figure 4 illustrates the deposition of a 3.9 μm aerosol in each component of the NIV system at 30 LPM and the resulting changes in DE associated with streamlining. For the T-connector, the streamlined design dramatically reduces deposition in the entrainment region by reducing both recirculation and turbulence. The resulting 7.2% DE in the SLp-10-T model represents a reduction in DE from the base design (32.5%) by a relative percent difference of −80%, or a factor of 4.5×. Considering the cannulas, the SL-10-CL design clearly reduces deposition in the nasal prongs compared with the Base-10-CL model. The result is a reduction in deposition efficiency by a relative percent difference of −45.6% for 3.9 μm droplets at 30 LPM. Still, approximately 20% deposition in the streamlined cannula is observed to occur mostly at the location of diameter reduction from 10 to 8 mm and the dividing point of the nasal prongs. It appears that further streamlining of these features could result in even lower deposition efficiency in the cannula.

Figure 5 illustrates localized deposition efficiencies for the case of 4.7 μm droplets at 45 LPM. For these conditions, the SL-10-T design (Figure 5b) remains highly effective at delivering the aerosol with a DE of only 8.4% and a relative percent difference of approximately −80% compared with Case 1 (Figure 5a). Some increased recirculation is evident in the streamlined T-connector, as indicated by additional deposition sites, which may influence performance if the flow rate is increased further. Considering the streamlined nasal cannula (Figure 5d), increased deposition is observed in the prongs compared with the same component at 30 LPM and 3.9 μm droplets. However, compared with the base model and same droplet conditions, the SL-10-CL design reduces DE by a relative percent difference of approximately −25%.

Figure 6 illustrates emitted dose for Cases 1–3 at two flow rates for particle sizes of 3.9 and 4.7 μm based on CFD simulations. For all cases, increasing the flow rate from 30 to 45 LPM reduces emitted dose by 3-fold for Case 1 and 2-fold for Cases 2 and 3. Decreasing the aerosol size from 4.7 to 3.9 μm increases the emitted dose by a factor of approximately 1.5. For a 3.9–4.7 μm aerosol at 30 LPM, use of the streamlined designs increases emitted dose by a factor of 1.6–2.1, which is consistent with the experimentally determined values. Similarly for a 3.9–4.7 μm aerosol at 45 LPM, use of the streamlined designs increased emitted dose by a factor of 2.5–2.8 based on CFD predictions.

DISCUSSION

NIV is growing in popularity based on positive clinical outcomes and a reduction in patient risk compared with invasive mechanical ventilation.[16,36] Clearly, patients with compromised airways requiring NIV may also benefit from medical aerosol delivery. Several decades of research have resulted in techniques and best practices that enable aerosol administration during NIV with delivery rates that are typically below 10% in adults.[8–11,17,38,44] Nasal high flow therapy is one form of NIV that is resulting in promising clinical outcomes with the use of only a simple nasal cannula interface.[37,39,41,42] However,

previous studies have not considered the delivery efficiency of a conventional-sized aerosol from the site of formation through a cannula interface at flow rates typical of nasal HFT in adults. Based on the high flow rates and narrow flow passages of nasal HFT with conventional droplet sizes, it would be reasonable to guess that all of the aerosol is lost in the delivery circuit and that drug does not actually reach the patient.

One outcome of this study is the quantification of aerosol delivery from a model steady state HFT setup at multiple flow rates using commercial (or base) components. Both the *in vitro* and CFD results indicate that for a 10 mm T-connector, 10 mm tubing, and large bore (medium size) Optiflow nasal cannula, approximately 10–20% of the aerosol is emitted from the cannula. Using a smaller 3.9 μm aerosol, which could not be generated with the mesh nebulizer used in this study, CFD predictions indicate that 30% of the dose is emitted from the base component system at a flow rate of 30 LPM. These steady state delivered dose values are higher than expected for typical NIV systems and will likely be reduced in the presence of realistic breath profiles.

A second outcome of the current study is a demonstration that streamlining NIV circuit components can be used to dramatically reduce deposition and increase the emitted dose. Streamlined designs reduced deposition in the T-connector by a relative percent difference of approximately −70%, or a 4-fold reduction in deposition. In the nasal cannula, the streamlined designs reduced deposition losses by a percent difference of approximately −15% to −20%. The depositional loss fractions remained high in the connective tubing due to impaction and sedimentation of the conventional-sized aerosol. As a result of large reductions in component deposition, the emitted dose of the streamlined systems was increased. Specifically, streamlined designs increased the emitted dose compared with Case 1 by a relative percent difference of approximately 60% based on *in vitro* experiments. In the CFD predictions, the highest emitted dose was 50% for a 3.9 μm aerosol at 30 LPM. Considering CFD results for two particle sizes (3.9 and 4.7 μm) and flow rates of 30 and 45 LPM, the streamlined designs produced a 1.6 to 2.8 fold increase in delivery.

The focus of this study was to analyze and improve the delivery of conventional sized aerosols during nasal HFT by implementing a streamlining approach. Typical flow rates associated with nasal HFT are in the range of 20–45 LPM with flow rates as high as 60 LPM. Poor performance of the base component system is likely because the T-connector was designed for lower neonatal flow rates and the Optiflow cannula was not designed for aerosol delivery. Higher flow T-connectors have a 22 mm line size, which is not consistent with nasal ventilation gas delivery. All other nasal cannulas have very small nasal prong internal diameters (~2 mm), which are not practical for aerosol delivery at high flow rates. Emitted dose may be improved some with the generation of an even smaller aerosol. However, mesh nebulizers have a number of advantages and are currently very popular for both pediatric and adult patients.[11,43] The mesh nebulizer selected is known to produce the smallest aerosol in the Aeroneb line of devices.[26] As a result of these observations, the base component system selected represents a practical best case taken from existing components that would likely be implemented in clinical use. Results indicate that the streamlined components can be used to dramatically reduce depositional losses and increase emitted dose compared with the base component system. Other approaches to improve the delivery of the base components include using a smaller particle size and reducing the flow rate. With both of these approaches, the streamlined design is still expected to perform better on a relative basis. Reducing the flow rate significantly to improve delivery changes the system from nasal HFT, and interrupts the ventilator support that the patient receives. Furthermore, previous studies do not indicate improved delivery from commercial systems with the use of different conventional nebulizers and very low flow rates.[3,4]

Results of this study illustrate the advantages of streamlined designs for respiratory drug delivery during mechanical ventilation; however, the approach taken to produce these designs may vary. In aerosol science, correlations exist that describe the inertial deposition of particles in curved tubes and bifucations.[5,32,40] These correlations may be used to decrease deposition in certain components of the delivery system. However, they are not practical for predicting deposition in the complex T-connections and cannula geometries considered in this study. Instead, CFD was implemented to understand the fluid dynamics affecting deposition within the components and then to test a series of prototype models that minimize deposition. The implementation of CFD for understanding droplet or particle losses in aerosol delivery was previously reviewed by Longest and Holbrook.[24] Longest and Hindle[21] described a quantitative analysis and design (QAD) approach in which CFD was implemented to develop design correlations for minimizing inhaler deposition as a function of transport characteristics. In the current study, insight gained from the CFD simulations was used to iteratively modify and minimize deposition, which led to the proposed streamlined designs. Future studies may implement CFD to employ a more quantitative approach for design optimization, such as the QAD method.

Based on the results of this study, it appears that streamlined geometries offer an effective method to significantly improve the delivery of aerosols through components of NIV systems. The streamlining approach does not require additional technology to be added to the aerosol generation system. By simply replacing the circuit components that are most responsible for depositional loss with streamlined versions, drug delivery to the patient can be increased approximately 2-fold. This increase in delivery efficiency is likely important for new inhaled medications with narrow therapeutic windows, increased costs, and long delivery times, such as aerosolized iloprost. Increasing the dose emitted from the delivery circuit will directly reduce the required administered dose, delivery time, and expense. It is not expected that the streamlined components will adversely influence gas delivery. In fact, the reduced velocities of the streamlined nasal cannula prongs may be more comfortable to the patient at the high flow rates employed with NIV.

Limitations of the current study include operation at room temperature conditions, steady flow without downstream cyclic breathing, lack of a nasal geometry, one configuration of the connective tubing, and use of the Aeroneb Lab nebulizer, rather than the commercial version. Typical nasal HFT systems operate at 32–37 °C with >90% RH and include either a water jacketed line or wire heater to maintain temperature and prevent supersaturation and rainout of the humidity. Near-saturated conditions were implemented in the current system; however, supersaturation and “rain-out” were prevented by matching the room and gas delivery temperatures. As a result, the size of the aerosol is not expected to change due to condensation or evaporation. Nasal HFT is delivered at a steady state or constant flow rate, which is consistent with the *in vitro* model. However, nasal inhalation and exhalation at the cannula interface was absent and may influence deposition and the dose delivered to the patient. As described in previous publications, the nasal geometry will filter an additional portion of the aerosol before it reaches the lungs.[27] As a result, actual lung delivery fractions will be lower than the emitted dose values in the current study. The connective tubing configuration with a 90° bend was intended to maximize aerosol deposition both in the tube and cannula. However, other configurations may influence the reported delivery values. Finally, the Aeroneb Lab nebulizer is currently not approved for human use. The commercially available Aeroneb Pro and Solo devices are expected to have larger MMAD values[1,19,26] and therefore reduced emitted doses compared with the results of this study.

An additional limitation of the CFD model implemented in this study was the assumption of a monodisperse aerosol equal to the MMAD of the initial aerosol exiting the nebulizer. Droplets were also assumed not to evaporate, which is reasonable for the isothermal

experimental system. However, in the experiments deposition of the polydisperse aerosol throughout the system will change the MMAD as larger particles are selectively filtered in the upstream components. Separate experiments were conducted with the Aeroneb Lab nebulizer and a different formulation producing an aerosol with an initial MMAD of 4.8 μm. After this aerosol was passed through the Base-10-T and SL-10-CL geometries, the exiting MMAD was 2.9 μm. As a result, it is expected that CFD with a monodisperse 4.7 μm aerosol should over predict deposition in the tubing and cannula, which was observed in the comparisons with experimental results. The CFD model also neglected the potential for resuspension of droplets or particles from the model surface. This is reasonable based on the particle size and flow rates considered unless significant condensation (or rain-out) occurs in the physical model.

Based on these results, delivery rates of 40–50% with conventional-sized aerosols can be achieved during NIV. However, deposition will remain high in the connective tubing. Deposition can be further reduced by additional changes to the cannula design, as observed in the Results. However, a practical minimum deposition efficiency in the nasal cannula for conventional aerosols at flow rates of ~30 LPM is likely 10–20%. Also, nasal deposition will reduce the lung delivered dose. At 30 LPM, the Stokes number of the particles entering the nostrils based on hydraulic diameters of the cannula outlets are 0.172 for the base case and 0.097 for the streamlined case. These Stokes numbers will likely result in high depositional losses in the nasal passage; however, the nasal deposition with the streamlined case is expected to be much less than the unaltered design based on the reduced Stokes number.

The practical limitations of line deposition and loss in the nasal cavity can be overcome by using submicrometer aerosols and divided stream ECG nasal delivery, as previous reported.[27,30] The ECG approach can deliver over 90% of an aerosol from the site of droplet formation (i.e., the nebulizer) to the lungs in a steady state delivery mode. However, the goal of the current study was to explore reductions in depositional losses and increases in emitted dose for conventional aerosol sizes by a logical redesign of the nasal HFT system components. The result that emitted dose can be improved approximately 2-fold without additional complexity in the delivery system appears promising.

CONCLUSIONS

Streamlining components of the NIV delivery system was observed to largely reduce deposition in individual components and increase emitted dose of aerosolized medications. Compared with a NIV system of commercial components, streamlined designs reduced aerosol depositional loss within individual components by up to 4-fold and increased emitted dose by a factor of approximately 2-fold. Therefore, these redesigned components provide a low cost solution that is capable of significantly improving aerosol delivery rates during NIV. These improved delivery rates may not be required for currently successful inhaled medications with broad therapeutic windows, like bronchodilators. However, increasing the delivery efficiency by a multiple of 2 is important for medications with high costs, significant side effects, narrow therapeutic windows, or long delivery times. In this study, a model nasal HFT system is used as a characteristic case to demonstrate the benefits of the streamlining approach for improving aerosol delivery during mechanical ventilation. The same concept can directly be applied to other NIV systems, like CPAP, and to aerosol delivery during invasive mechanical ventilation with endotracheal tubes. Further testing of the components developed in this study is needed during active breathing and for different aerosol sizes, delivery flow rates, and tubing configurations.

Acknowledgments

This study was supported by Award R01 HL107333 from the National Heart, Lung, and Blood Institute. The content is solely the responsibility of the authors and does not necessarily represent the official views of the National Heart, Lung, And Blood Institute or the National Institutes of Health.

ABBREVIATIONS

ACI	Andersen cascade impactor
CFD	Computational fluid dynamics
CL	cannula
COPD	chronic obstructive pulmonary disease
CPAP	continuous positive airway pressure
DE	deposition efficiency
DF	deposition fraction
ECG	enhanced condensational growth
HFT	high flow therapy
HPLC	high-performance liquid chromatography
IF	inlet fraction of aerosol
LES	large eddy simulation
LPM	liters per minute
LRN	Low Reynolds number
MMAD	mass median aerodynamic diameter
NIV	non-invasive ventilation
RH	relative humidity
SL	streamlined
SLf	streamlined with fins
SLp	streamlined with perforated plate
UV	ultraviolet

References

1. Abdelrahim ME, Chrystyn H. Aerodynamic characteristics of nebulized terbutaline sulphate using the next generation impactor (NGI) and CEN method. Journal of Aerosol Medicine and Pulmonary Drug Delivery. 2009; 22(1):19–28. [PubMed: 19392586]
2. Ari A, Fink JB. Inhalation Therapy in Patients Receiving Mechanical Ventilation: An Update. Journal of Aerosol Medicine and Pulmonary Drug Delivery. 10.1089/jamp.2011.0936 2012
3. Ari A, Harwood R, Sheard M, Dailey P, Fink JB. In vitro comparison of heliox and oxygen in aerosol delivery using pediatric high flow nasal cannula. Pediatric Pulmonology. 2011; 46(8):795–801. [PubMed: 21438178]
4. Bhashyam AR, Wolf MT, Marcinkowski AL, Saville A, Thomas K, Carcillo JA, Corcoran TE. Aerosol delivery through nasal cannulas: An in vitro study. Journal of Aerosol Medicine and Pulmonary Drug Delivery. 2008; 21(2):181–187. [PubMed: 18518794]
5. Cheng YS, Wang CS. Motion of particles in bends of circular pipes. Atmospheric Environment. 1981; 15:301–306.

6. Crowe CT, Troutt TR, Chung JN. Numerical models for two-phase turbulent flows. Annual Review of Fluid Mechanics. 1996; 28:11–43.
7. Dewan NA, Bell CW. Effect of low flow and high flow oxygen delivery on exercise tolerance and sensation of dyspnea. A study comparing the transtracheal catheter and nasal prongs. Chest. 1994; 105:1061–1065. [PubMed: 8162725]
8. Dhand R. New Frontiers in Aerosol Delivery During Mechanical Ventilation. Respiratory Care. 2004; 49:666–677. [PubMed: 15165301]
9. Dhand R. Inhalation therapy in invasive and noninvasive mechanical ventilation. Current Opinion in Critical Care. 2007; 13:27–38. [PubMed: 17198046]
10. Dhand R. Aerosol delivery during mechanical ventilation: From basic techniques to new devices. Journal of Aerosol Medicine and Pulmonary Drug Delivery. 2008; 21(1):45–60. [PubMed: 18518831]
11. Dhand R. Aerosol therapy in patients receiving noninvasive positive pressure ventilation. Journal of Aerosol Medicine and Pulmonary Drug Delivery. 2012; 25(2):63–78. [PubMed: 22191396]
12. Dysart K, Miller TL, Wolfson MR, Shaffer TH. Research in high flow therapy: Mechanisms of action. Respiratory Medicine. 2009; 103:1400–1405. [PubMed: 19467849]
13. Ghalichi F, Deng X, Champlain AD, Douville Y, King M, Guidoin R. Low Reynolds number turbulence modeling of blood flow in arterial stenoses. Biorheology. 1998; 35(4&5):281–294. [PubMed: 10474655]
14. Gosman AD, Ioannides E. Aspects of computer simulation of liquid-fueled combustors. Journal of Energy. 1981; 7:482–490.
15. Hasan MA, Lange CF. Estimating in vitro airway surface liquid concentration in trials of inhaled antibiotics. Journal of Aerosol Medicine. 2007; 20(3):282–293. [PubMed: 17894535]
16. Hess DR. The evidence for noninvasive positive-pressure ventilation in the care of patients in acute respiratory failure: a systematic review of the literature. Respiratory Care. 2004; 49:810–829. [PubMed: 15222912]
17. Hess DR. The mask of noninvasive ventilation: Principles of design and effects on aerosol delivery. Journal of Aerosol Medicine. 2007; 20:S85–S99. [PubMed: 17411410]
18. Ivri, E.; Fink, J. Aerosol delivery apparatus and method for pressure-assisted breathing systems. United States Patent No. 7,290,541 B2. 2007.
19. Kuhli M, Weiss M, Steckel H. A sampling and dilution system for droplet aerosols from medical nebulisers developed for use with an optical particle counter. Aerosol Science. 2009; 40:523–533.
20. Longest PW, Hindle M. Evaluation of the Respimat Soft Mist inhaler using a concurrent CFD and in vitro approach. Journal of Aerosol Medicine and Pulmonary Drug Delivery. 2009; 22(2):99–112. [PubMed: 18956950]
21. Longest PW, Hindle M. Quantitative analysis and design of a spray aerosol inhaler. Part 1: Effects of dilution air inlets and flow paths. Journal of Aerosol Medicine and Pulmonary Drug Delivery. 2009; 22(3):271–283. [PubMed: 19466904]
22. Longest PW, Hindle M, Das Choudhuri S, Byron PR. Numerical simulations of capillary aerosol generation: CFD model development and comparisons with experimental data. Aerosol Science and Technology. 2007; 41:952–973.
23. Longest PW, Hindle M, Das Choudhuri S, Xi J. Comparison of ambient and spray aerosol deposition in a standard induction port and more realistic mouth-throat geometry. Journal of Aerosol Science. 2008; 39:572–591.
24. Longest PW, Holbrook LT. In silico models of aerosol delivery to the respiratory tract - Development and applications. Advanced Drug Delivery Reviews. 2012; 64:296–311. [PubMed: 21640772]
25. Longest PW, Kleinstreuer C, Buchanan JR. Efficient computation of micro-particle dynamics including wall effects. Computers & Fluids. 2004; 33(4):577–601.
26. Longest PW, Spence BM, Holbrook LT, Mossi KM, Son YJ, Hindle M. Production of inhalable submicrometer aerosols from conventional mesh nebulizers for improved respiratory drug delivery. Journal of Aerosol Science. 2012; 51:66–80. [PubMed: 22707794]
27. Longest PW, Tian G, Hindle M. Improving the lung delivery of nasally administered aerosols during noninvasive ventilation - An application of enhanced condensational growth (ECG).

Journal of Aerosol Medicine and Pulmonary Drug Delivery. 2011; 24(2):103–118. 110.1089/jamp.2010.0849. [PubMed: 21410327]

28. Longest PW, Vinchurkar S. Effects of mesh style and grid convergence on particle deposition in bifurcating airway models with comparisons to experimental data. Medical Engineering and Physics. 2007; 29(3):350–366. [PubMed: 16814588]
29. Longest PW, Vinchurkar S. Validating CFD predictions of respiratory aerosol deposition: effects of upstream transition and turbulence. Journal of Biomechanics. 2007; 40:305–316. [PubMed: 16533511]
30. Longest PW, Walenga RL, Son Y-J, Hindle M. High efficiency generation and delivery of aerosols through nasal cannula during noninvasive ventilation. Journal of Aerosol Medicine and Pulmonary Drug Delivery. 2013 In press.
31. Longest PW, Xi J. Effectiveness of direct Lagrangian tracking models for simulating nanoparticle deposition in the upper airways. Aerosol Science and Technology. 2007; 41:380–397.
32. Martonen TB. Mathematical model for the selective deposition of inhaled pharmaceuticals. Journal of Pharmaceutical Sciences. 1993; 82(12):1191–1199. [PubMed: 8308694]
33. Matida EA, Finlay WH, Grgic LB. Improved numerical simulation of aerosol deposition in an idealized mouth-throat. Journal of Aerosol Science. 2004; 35:1–19.
34. Matida EA, Nishino K, Torii K. Statistical simulation of particle deposition on the wall from turbulent dispersed pipe flow. International Journal of Heat and Fluid Flow. 2000; 21:389–402.
35. Morsi SA, Alexander AJ. An investigation of particle trajectories in two-phase flow systems. Journal of Fluid Mechanics. 1972; 55(2):193–208.
36. Nava S, Hill NS. Non-invasive ventilation in acute respiratory failure. Lancet. 2009; 374:250–259. [PubMed: 19616722]
37. Parke RL, McGuinness SP, Eccleston ML. A Preliminary Randomized Controlled Trial to Assess Effectiveness of Nasal High-Flow Oxygen in Intensive Care Patients. Respiratory Care. 2011; 56(3):265–270. [PubMed: 21255498]
38. Parkes SN, Bersten AD. Aerosol kinetics and bronchodilator efficacy during continuous positive airway pressure delivered by face mask. Thorax. 1997; 52(2):171–175. [PubMed: 9059480]
39. Price AM, Plowright C, Makowski A, Misztal B. Using a high-flow respiratory system (Vapotherm) within a high dependency setting. Nursing in Critical Care. 2008; 13(6):298–304. [PubMed: 19128313]
40. Pui DYH, Romay-Novas F, Liu BYH. Experimental study of particle depositon in bends of circular cross section. Aerosol Science and Technology. 1987; 7:301–315.
41. Rea H, McAuley S, Jayaram L, Garrett J, Hockey H, Storey L, O'Donnell G, Haru L, Payton M, O'Donnell K. The clinical utility of long-term humidification therapy in chronic airway disease. Respiratory Medicine. 2010; 104:525–533. [PubMed: 20144858]
42. Roca O, Riera J, Torres F, Masclans JR. High-Flow Oxygen Therapy in Acute Respiratory Failure. Respiratory Care. 2010; 55(4):408–413. [PubMed: 20406507]
43. Rubin BK. Pediatric aerosol therapy: New devices and new drugs. Respiratory Care. 2011; 56(9): 1411–1421. [PubMed: 21944688]
44. Sangwan S, Gurses BK, Smaldone GC. Facemasks and facial deposition of aerosols. Pediatric Pulmonology. 2004; 37(5):447–452. [PubMed: 15095329]
45. Vinchurkar S, Longest PW. Evaluation of hexahedral, prismatic and hybrid mesh styles for simulating respiratory aerosol dynamics. Computers and Fluids. 2008; 37:317–331.
46. Wilcox, DC. Turbulence Modeling for CFD. 2. DCW Industries, Inc; California: 1998.
47. Xi J, Longest PW, Martonen TB. Effects of the laryngeal jet on nano- and microparticle transport and deposition in an approximate model of the upper tracheobronchial airways. Journal of Applied Physiology. 2008; 104:1761–1777. [PubMed: 18388247]

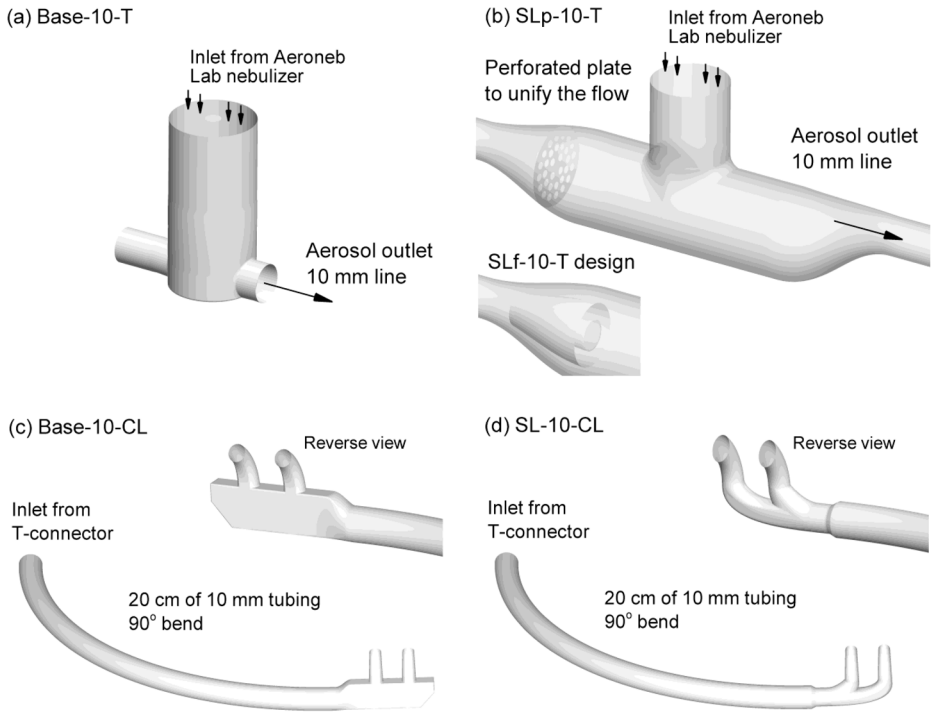

Figure 1.

Individual components of the noninvasive delivery system including the (a) commercial Aerogen Neonatal T-connector (Base-10-T), (b) streamlined mesh nebulizer T-connector (SLp-10-T), (c) commercial Optiflow nasal cannula, medium size (Base-10-CL), and (d) streamlined nasal cannula (SL-10-CL). In panel (b), the SLf-10-T design implements circular fins instead of a porous plate to unify the flow.

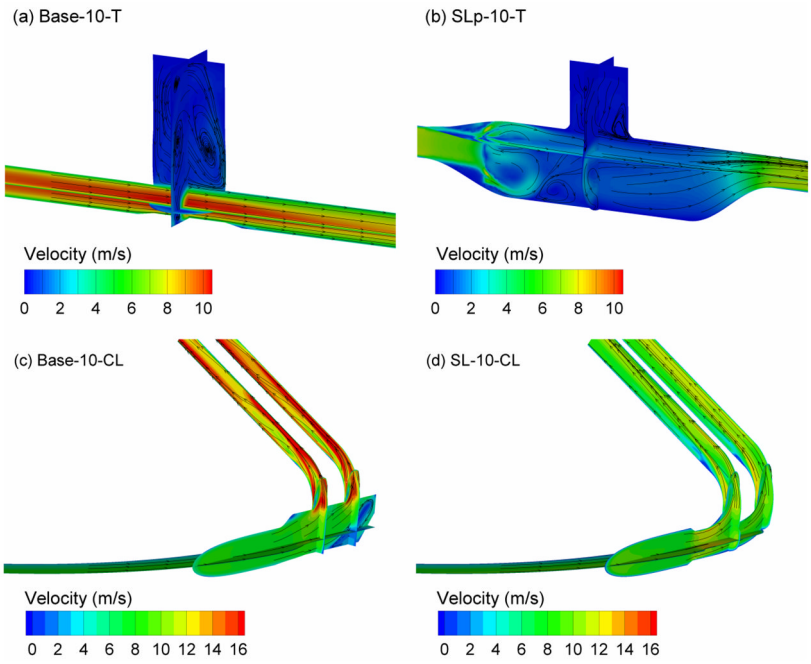

Figure 2.
Velocity fields presented as contours of magnitude and surface streamtraces on selected planes at a steady flow rate of 30 LPM for (a) Base-10-T, (b) SLp-10-T, (c) Base-10-CL, (d) SL-10-CL.

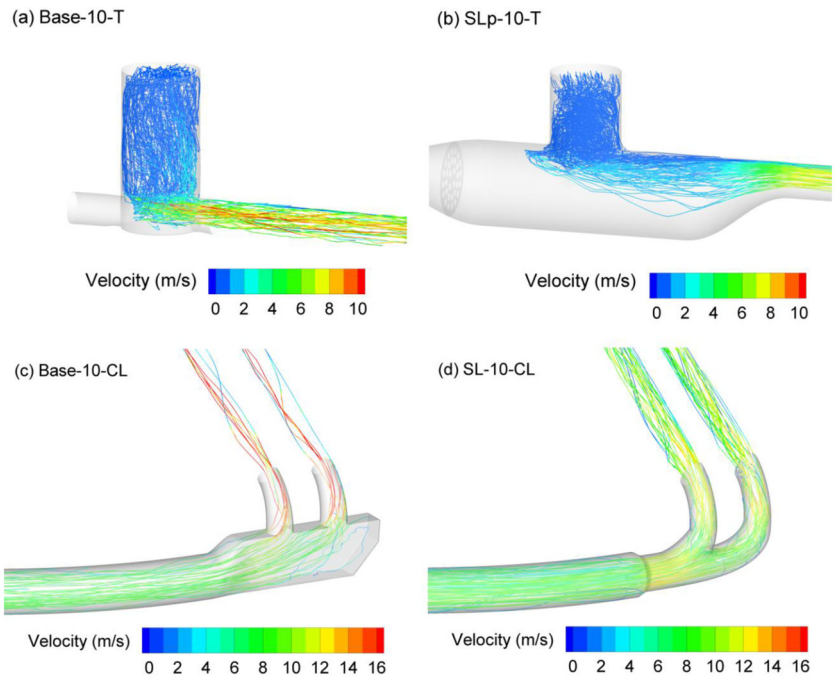

Figure 3.
Trajectories of 3.9 μm particles contoured according to local particle velocity at a steady flow rate of 30 LPM for (a) Base-10-T, (b) SLp-10-T, (c) Base-10-CL, (d) SL-10-CL.

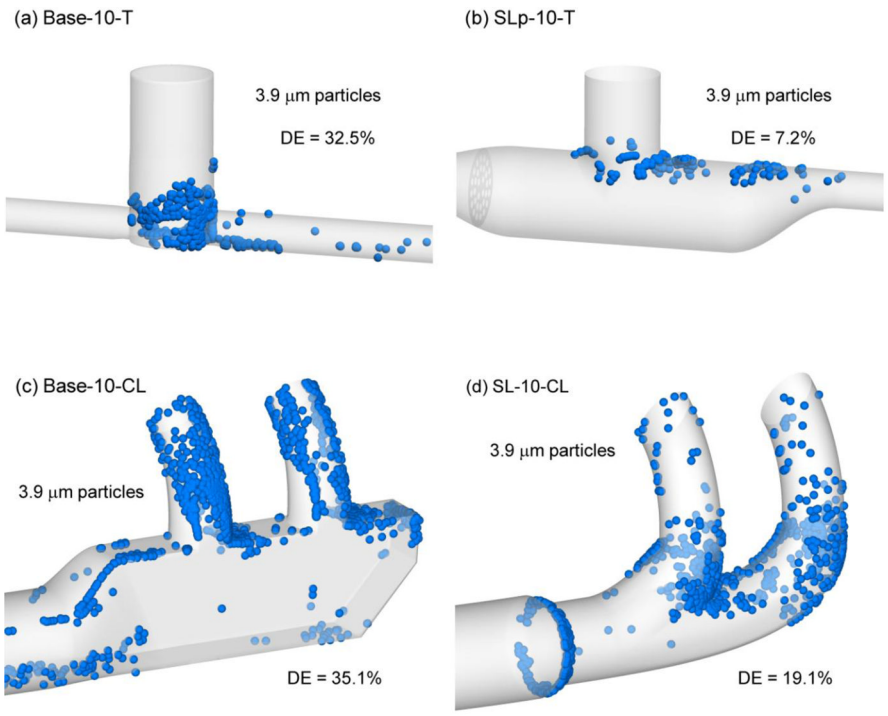

Figure 4.
Deposition locations of representative 3.9 μm particles and component deposition efficiencies (DEs) at a flow rate of 30 LPM for (a) Base-10-T, (b) SLp-10-T, (c) Base-10-CL, (d) SL-10-CL.

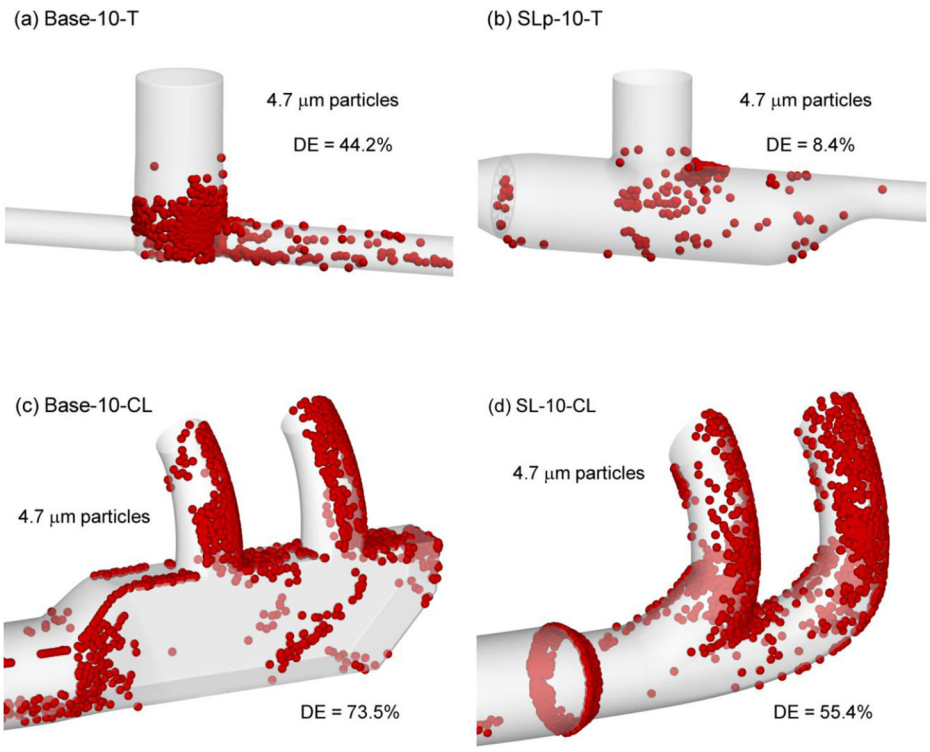

Figure 5.
Deposition locations of representative 4.7 μm particles and component deposition efficiencies (DEs) at a flow rate of 45 LPM for (a) Base-10-T, (b) SLp-10-T, (c) Base-10-CL, (d) SL-10-CL.

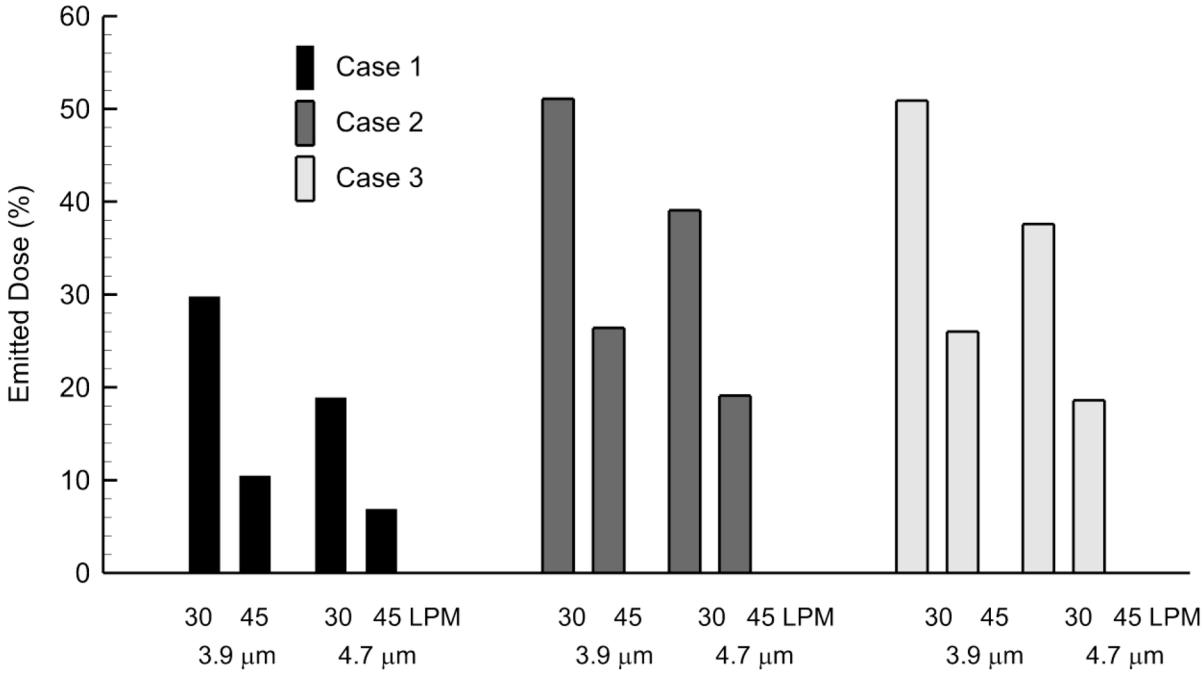

Figure 6.
Emitted dose of the drug aerosol (as a %) for Cases 1–3 at multiple flow rates (30 and 45 LPM) and particle sizes (3.9 and 4.7 μm) based on CFD predictions.

Table 1

Combinations of commercial (base) and streamlined (SL) T-connectors, tubing, and cannulas to form NIV cases.

	Flow rate (LPM)	T-connector	Tubing	Cannula
Case 1	30 and 45	Base-10-T	20 cm of 10 mm tubing	Base-10-CL
Case 2	30 and 45	SLp-10-T	20 cm of 10 mm tubing	SL-10-CL
Case 3	30 and 45	SLf-10-T	20 cm of 10 mm tubing	SL-10-CL
Case 4	30 and 45	SLp-10-T	20 cm of 10 mm tubing	Base-10-CL

Abbreviations: 10, 10 mm tubing; Base, commercially available base case unit; CL, cannula; f, fin design; p, perforated plate design; SL, streamlined; T, T-connector

Table 2

Experimental results of deposition fractions (DF) as a percentage of nominal dose presented as mean (SD) values for a steady flow rate of 30 LPM.

	Nebulizer DF (%)	T-Connector DF (%)	20 cm of tubing DF (%)	Cannula DF (%)	Total device DF[a] (%)	Emitted Dose (%)
Case 1	7.1 (5.4)[b]	30.6 (1.9)	19.0 (0.6)	15.4 (3.0)	72.1 (6.2)	27.8 (6.1)
Case 2	4.9 (2.0)	5.7 (0.4)	27.2 (2.2)	18.3 (1.1)	56.1 (2.6)	44.0 (2.6)
Case 3	6.4 (1.1)	5.1 (2.4)	32.8 (4.0)	16.8 (1.6)	61.1 (4.4)	38.9 (4.4)
Case 4	5.1 (2.0)	5.1 (1.3)	30.3 (9.0)	26.2 (2.6)	66.7 (7.4)	33.3 (7.4)

[a]Sum of component DF values.

[b]SD based on n = 4 experiments.

Table 3

Experimental deposition results converted to deposition efficiencies (DE) in each component, emitted dose, and relative percent difference compared with Case 1 for a flow rate of 30 LPM.

	Nebulizer + T-Connector DE (%)	20 cm of tubing DE (%)	Cannula DE (%)	Emitted Dose (%)
Case 1	37.7	30.5	35.6	27.8
Case 2	10.6	30.4	29.4	44.0
% Difference vs. Case 1	−71.9[a]	−0.3	−17.4	58.3[b]
Case 3	11.5	37.1	30.1	38.9
% Difference vs. Case 1	−69.5	21.6	−15.4	39.9
Case 4	10.2	33.7	43.9	33.3
% Difference vs. Case 1	−72.9	10.5	23.3	19.8

[a] Calculated as $(DE_{Case\ 2}-DE_{Case\ 1})/DE_{Case\ 1} \times 100$. Positive values indicate an increase relative to Case 1.

[b] Maximum percent difference indicating a ~60% improvement in drug delivery for Case 2 compared with Case 1 based on *in vitro* measured results.

Table 4

Comparison of experimental and CFD results based on DEs in each component and emitted doses for the entire system with a flow rate of 30 LPM.

	Nebulizer + T-Connector DE (%)	20 cm of tubing DE (%)	Cannula DE (%)	Emitted dose (%)
Case 1				
Experiment	37.7	30.5	35.6	27.8
CFD[a]	36.5	38.3	51.9	18.9
% Difference[b]	−3.2	25.6	45.8	−32.0
Case 2				
Experiment	10.6	30.4	29.4	44.0
CFD	7.0	38.3	31.9	39.1
% Difference	−34.0	26.0	8.5	−11.1
Case 3				
Experiment	11.5	37.1	30.1	38.9
CFD	10.5	38.3	31.9	37.6
% Difference	−8.7	3.2	6.0	−3.3

[a] CFD results are for a monodisperse 4.7 μm aerosol, which provided an adequate monodisperse estimate to the experimental data across multiple components.

[b] Calculated as $(DE_{CFD} - DE_{in\ vitro})/DE_{in\ vitro} \times 100$.